Probing color-singlet exchange in $Z+2$-jet events at the CERN LHC

D. Rainwater
Department of Physics, University of Wisconsin, Madison, Wisconsin 53706

R. Szalapski
Theory Group, KEK, 1-1 Oho, Tsukuba, Ibaraki 305, Japan

D. Zeppenfeld
Department of Physics, University of Wisconsin, Madison, Wisconsin 53706
(Received 30 May 1996)

The purely electroweak process $qq \to qqZ$ (via t-channel γ/Z or W exchange) provides a copious and fairly clean source of color-singlet exchange events in pp collisions at the CERN LHC. A judicious choice of phase-space region allows the suppression of QCD backgrounds to the level of the signal. The color-singlet-exchange signal can be distinguished from QCD backgrounds by the radiation patterns of additional minijets in individual events. A rapidity-gap trigger at the minijet level enhances substantially the signal versus the background. Analogous features of weak-boson scattering events make $Z+2$-jet events at the CERN LHC an ideal laboratory for investigation of the soft-jet activity expected in weak-boson scattering events. [S0556-2821(96)03023-8]

PACS number(s): 13.87.Ce, 12.38.Bx, 14.70.Hp

I. INTRODUCTION

The study of weak-boson scattering events and the search for a heavy Higgs boson will remain among the most important tasks of the CERN Large Hadron Collider (LHC) as long as the origin of the spontaneous breakdown of the electroweak $SU(2)\times U(1)$ gauge symmetry has not been established by experiment. Consequently, much work has been devoted in recent years on devising methods for the separation of weak-boson scattering events, i.e., the purely electroweak process $qq \to qqVV$, from background events such as weak-boson pair production or top-quark decays. One such technique is forward jet tagging, the requirement to observe one or both of the two forward quark jets of the $qq \to qqVV$ process [1–3]. However, additional characteristics of the signal must be employed to suppress backgrounds.

In a weak-boson scattering event, no color is exchanged between the initial-state quarks. Color coherence between initial- and final-state gluon bremsstrahlung then leads to a suppression of hadron production in the central region, between the two tagging-jet candidates of the signal [4]. This is in contrast with most background processes which typically involve color exchange in the t channel and thus lead to enhanced particle production in the central region. It was hoped that the resulting rapidity gaps in signal events (large regions in pseudorapidity without observed hadrons) could be used for background suppression. Unfortunately, in pp collisions at $\sqrt{s}=14$ TeV at the CERN LHC, the low-signal cross sections require running at high luminosity, and then overlapping events in a single bunch crossing will likely fill a rapidity gap even if it is present at the level of a single pp collision. The different color structures of signal and background processes can be exploited even at high luminosity, however, if one defines rapidity gaps in terms of minijets (of transverse momenta in the 20–50 GeV range) instead of soft hadrons [5].

Sizable background reductions via a minijet veto require the lowering of jet-energy thresholds to a range where the probability for additional parton emission becomes order unity. In a perturbative calculation, the resulting condition, $\sigma(n+1\text{jets}) \approx \sigma(n\text{jets})$, indicates that one is leaving the validity range of fixed-order perturbation theory, and it becomes difficult to provide reliable theoretical estimates of minijet emission rates. Gluon emission is governed by very different scales in signal as compared to background processes, due to their different color structures. Thus a parton shower approach cannot be expected to give reliable answers either unless both color coherence and the choice of scale are implemented correctly, for which additional information is needed.

In this paper we describe why and how a different process, Zjj production with subsequent $Z \to \ell^+\ell^-$ decay, can be used to answer experimentally these questions at the CERN LHC in a region of phase space very similar to the one relevant for weak-boson scattering. The dominant source of Zjj events is the $O(\alpha_s^2)$ QCD correction to Drell-Yan production. These events involve color exchange between incident partons, similar to the QCD backgrounds to weak-boson scattering events. In addition, there are electroweak sources of Zjj events; namely, processes of the type $qq \to qqZ$ which proceed via color-singlet γ, Z, or W exchange. The W-exchange process includes the fusion of two virtual W's to a Z boson, as shown in Fig. 1(e), and thus is very similar to Higgs-boson production via weak-boson fusion. By tagging the two forward quark jets and requiring a large rapidity separation between the two, the QCD background can be reduced to the level of the signal, or even below. It thus becomes possible to study minijet emission in electroweak and QCD Zjj production separately and to obtain the necessary experimental information for correct modeling of multiple parton emission in t-channel color-singlet and color-octet exchange.

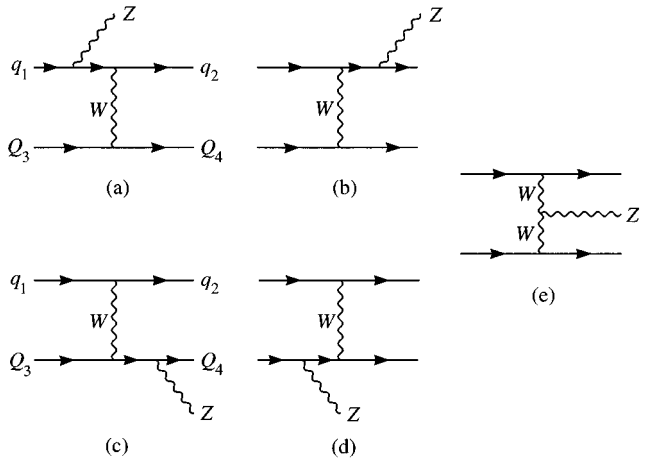

FIG. 1. Feynman graphs for Zjj production via charged-current exchange. The WW-fusion graph (e) simulates weak-boson scattering processes.

Our analysis is based on full tree-level Monte Carlo programs at the parton level. We start out in Sec. II by describing these tools. Simulating the minijet emission in Zjj events requires a calculation of $Z+3$-jet cross sections. While the QCD backgrounds [6–8] and the Zjj signal process [9] have been available in the literature, we here present a first calculation of electroweak $qq\to qqZg$ production (and crossing related processes). In Sec. III, using the Zjj programs, we identify forward-jet-tagging criteria which lower the QCD backgrounds to approximately the level of the signal. We also show how tagging-jet and decay-lepton distributions can be used to separate the signal from the background on a statistical basis [9,10].

Having defined the hard scattering processes to be investigated, we then turn to the different minijet patterns in signal and background events in Sec. IV. Two characteristics differentiate between signal and QCD background, the angular distribution of minijets and their typical transverse momenta. We discuss the probability for finding minijets in hard Zjj events and describe how this probability and the minijet multiplicity depend on the phase space region of the hard scattering event. Final conclusions are then drawn in Sec. V.

II. CALCULATIONAL TOOLS

Two aspects of minijet (or soft-gluon) emission in Zjj production need to be modeled correctly in order to describe soft-jet activity in these hard-scattering events: the angular distribution of soft emitted partons which reflects the color coherence specific to the underlying hard scattering event, and the momentum scale governing soft-gluon emission. Both aspects are taken correctly into account by using full tree-level matrix elements for all subprocesses which contribute to $Zjjj$ production.

A. The $qq\to qqZ(g)$ signal process

Our basic signal process is Z bremsstrahlung in quark–(anti)quark scattering via W, Z, or photon exchange,

$$qQ\to qQZ,\quad Z\to\ell^+\ell^-\quad(\ell=e,\mu) \tag{1}$$

and crossing related subprocesses. Subsequent leptonic Z decay allows identification of the signal. The lepton distributions and the tagging of the two (anti)quark jets provide a good discrimination against QCD backgrounds (see below). In the phase-space region of interest the charged-current (CC) process of Fig. 1 dominates over neutral-current (NC) exchange, mainly because of the larger coupling of the quarks to the W as compared to the photon and Z. The WWZ vertex in the Feynman graph of Fig. 1(e) then leads to a contribution which resembles very closely Higgs-boson production in weak-boson scattering, $qq\to qqH$, and thus our signal process becomes a laboratory for studying QCD aspects of weak-boson scattering.

We use the results of Ref. [9] for our calculation of the $qq\to qq\ell^+\ell^-$ signal. All CC and NC subprocesses are added, and finite Z-width effects are included. When requiring a large rapidity separation between the two quark jets (tagging jets), the resulting large dijet invariant mass suppresses severely any s-channel processes which might give rise to the dijet pair. We, therefore, consider only t-channel weak-boson exchange. Also note that graphs with s-channel electroweak-boson exchange involve color exchange between the incident partons and have a counterpart in the QCD backgrounds to be considered below, but with electroweak-boson exchange replaced by gluon exchange, i.e., $(\alpha/2\sin^2\theta_W)^2\approx 2.8\times 10^{-4}$ replaced by $\alpha_s^2\approx 1.4\times 10^{-2}$. Thus the electroweak s-channel processes may be considered as a minor correction to the QCD backgrounds.

In order to determine the minijet activity in signal events, we need to evaluate the $O(\alpha_s)$ real parton emission corrections to the signal. We have performed a first calculation of the $O(\alpha^4\alpha_s)$ subprocess

$$qQ\to qQg\ell^+\ell^- \tag{2}$$

and all crossing related subprocesses. Production of the $\ell^+\ell^-$ pair via Z and γ exchange is considered. For CC processes, such as $us\to dcg\ell^+\ell^-$, 52 Feynman graphs contribute to Eq. (2); for NC processes 112 Feynman graphs need to be included. The resulting amplitudes are evaluated numerically using the techniques of Refs. [6,11] and have been checked against amplitudes generated with MadGraph [12]. The cross sections for the various subprocesses are evaluated and added in a Monte Carlo program[1] whose phase-space generator and overall normalization have been tested by comparing to an analogous $qQ\to qQgH$ generator [13].

B. The QCD $Zjj(j)$ background

Given the clean leptonic Z decay signature, the main background to electroweak $Z+n$-jet events arises from $O(\alpha_s^n)$ real emission QCD corrections to the Drell-Yan process $q\overline{q}\to Z\to\ell^+\ell^-$. For Zjj events these background processes include

$$q\overline{q}\to ggZ, \tag{3a}$$

[1]The code is available upon request from rain@pheno.physics.wisc.edu

TABLE I. Signal and background cross sections $B\sigma$ for $Zjj(j)$ events in pp collisions at $\sqrt{s}=14$ TeV. The two decay modes $Z\to e^+e^-,\mu^+\mu^-$ are considered. Results are given in units of fb after increasingly stringent cuts. The last column gives the ratio of signal to background cross section.

	Zjj signal	QCD Zjj background	S/B
Generic cuts [Eqs. (4)–(6)]	516	1.29×10^5	1:250
+ forward jet tagging, [Eqs. (7) and (8)]	86.6	627	1:7.2
+ $m_{jj}>1500$ GeV	44.2	87.9	1:2.0
+ $m_{jj}>2500$ GeV, $\Delta\eta_{\ell j}>1.6$	10.7	6.8	1.6:1
+ $p_{Tj}>100$ GeV	4.6	1.6	2.9:1

$$qg\to qgZ, \tag{3b}$$

or

$$qq\to qqZ \tag{3c}$$

via t-channel gluon exchange and all crossing related processes [18]. We shall call these processes the ''QCD Zjj'' background. The cross sections for the corresponding $Z+3$-jet processes, which we need for our modeling of minijet activity in the QCD Zjj background, have been calculated in Refs. [6–8]. Similar to the treatment of the signal processes, we use a parton-level Monte Carlo program based on the work of Ref. [7] to model the QCD Zjj and $Zjjj$ backgrounds.

For all our numerical results, we have chosen $\alpha_{\rm QED}=\alpha(M_Z)=1/128.93$, $M_Z=91.19$ GeV, and $G_F=1.16639\times10^{-5}$ GeV^{-2}, which translates into $M_W=79.97$ GeV and $\sin^2\theta_W=0.2310$ when using the tree-level relations between these input parameters. The running of the strong-coupling constant is evaluated at one-loop order, with $\alpha_s(M_Z)=0.12$. MRS A structure functions [14,15] are used throughout, and the factorization scale is chosen as the minimal transverse momentum of a defined jet in the event (see below). For the $qQ\to qQgZ$ signal, the scale of the strong coupling constant is taken to be the minimal transverse momentum of any of the three final state partons. For the $Zjj(j)$ QCD backgrounds, with $n=2$ and $n=3$ colored partons in the final state, the overall strong-coupling constant factors are taken as $(\alpha_s)^n=\Pi_{i=1}^n\alpha_s(p_{Ti})$, i.e., the transverse momentum of each additional parton is taken as the relevant scale for its production, irrespective of the hardness of the underlying scattering event. This procedure guarantees that the same α_s^2 factors are used for the hard part of a Zjj event, independent of the number of additional minijets, and at the same time the small scales relevant for soft-gluon emission are implemented.

Different scale choices or different input parameters will, of course, affect our numerical results. The use of leading order (LO) CTEQ 3L [or next-to-leading order (NLO) CTEQ 3M] distribution functions [16,15], for example, changes the cross-section values listed in the second row of Table I by approximately -4% $(+5\%)$. These small changes are much smaller than the uncertainties inherent to a tree level calculation and justify the use of NLO parton distribution functions in our LO calculations. Of more concern is the scale choice detailed above. A variation of the factorization and renormalization scales by a factor of two changes the 2-jet cross sections in the second row of Table I by about $\pm15\%$ for the signal and by about a factor 1.5 for the QCD background. Choosing the transverse mass of the Z as the scale leads to variations within the same range. Thus we expect the signal cross sections to be fairly well determined at leading order, similar to the analogous Higgs-boson production process by weak-boson fusion [17], while the much larger theoretical uncertainty for the background again emphasizes the need for experimental input.

III. Zjj EVENTS: ELECTROWEAK SIGNAL AND QCD BACKGROUNDS

Before analyzing the minijet activity in signal and background events, we need to identify the phase-space region for hard scattering events, $pp\to ZjjX$ with two hard jets in the final state. In a tree-level simulation, processes with exactly two final-state partons need to be considered for this purpose. In the actual experiments this would correspond to two-jet inclusive events. We are interested in electroweak Zjj production as a model process for weak-boson scattering. Thus we first need to identify the phase-space region where the WW-fusion graph of Fig. 1(e) becomes important. This question has been analyzed before for electroweak Wjj production at the Superconducting Super Collider (SSC), and we follow closely the procedure outlined in Ref. [10]. The acceptance cuts to be discussed below are chosen with the design of the ATLAS and Compact Muon Solenoid (CMS) detectors at the CERN LHC in mind [19].

The leptonic Z decay is a crucial part of the signal, and and we, therefore, consider events with two opposite-sign leptons, $\ell^+\ell^-=e^+e^-,\mu^+\mu^-$, of sufficient transverse momentum, in the central part of the detector, and well isolated from any jets:

$$p_{T\ell}>20\ \text{GeV},\quad |\eta_\ell|<2,$$
$$R_{\ell j}=\sqrt{(\eta_\ell-\eta_j)^2+(\phi_\ell-\phi_j)^2}>0.7. \tag{4}$$

Here η denotes the pseudorapidity and $R_{\ell j}$ is the lepton-jet separation in the pseudorapidity azimuthal-angle plane. In addition, the dilepton invariant mass must be consistent with Z decay:

$$m_Z-10\ \text{GeV}<m_{\ell\ell}<m_Z+10\ \text{GeV}. \tag{5}$$

In the following, unless stated otherwise, any parton satisfying the transverse momentum, pseudorapidity, and separation requirements

$$p_{Tj}>20\ \text{GeV},\quad |\eta_j|<5,\quad R_{jj}>0.7, \tag{6}$$

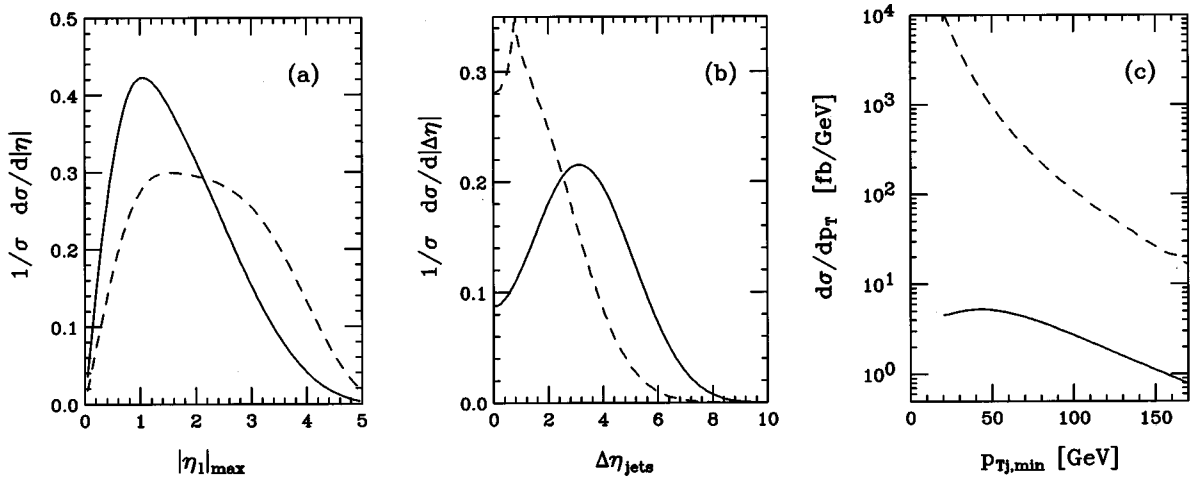

FIG. 2. Lepton and jet distributions of signal (solid lines) and background (dashed lines) Zjj events within the cuts of Eqs. (4)–(6). Shown are normalized distributions of (a) $|\eta_{\ell}|_{\max}$, the maximum lepton pseudorapidity, (b) the pseudorapidity separation $\Delta\eta_{\text{jets}}=|\eta(j_1)-\eta(j_2)|$ of the two jets, and (c) the differential cross section $d\sigma/dp_{Tj,\min}$, where $p_{Tj,\min}$ is the smaller of the two jet transverse momenta.

will be called a jet.

Event rates after these acceptance cuts are shown in the first row of Table I. Lepton and jet differential distributions for the signal (solid lines) and the background (dashed lines) are shown in Fig. 2. The lepton rapidity distribution of Fig. 2(a) shows that signal leptons are more centrally produced than those in QCD Zjj events. Concentrating on central leptons ($|\eta_{\ell}|<2$) does little harm to the signal while reducing the background by more than a factor of two. A stronger reduction of the background is achieved by exploiting the larger pseudorapidity separation of the two jets in the t-channel electroweak-boson exchange of the signal as compared to the QCD background [see Fig. 2(b)]. Finally, the transverse-momentum distribution of the softer of the two jets is shown in Fig. 2(c).

The large jet separation of the signal is typical also for weak-boson scattering events, and we, therefore, require at least three units of pseudorapidity between the jet definition cones of the two tagging jets. In addition, the leptons are required to occupy the pseudorapidity range between the two cones and the two tagging jets must fall into opposite hemispheres of the detector. With a cone radius of 0.7 for each of the jets, these conditions can be summarized as

$$|\eta_j^{\text{tag}\,1}-\eta_j^{\text{tag}\,2}|>4.4, \quad \eta_j^{\text{tag}\,1}\cdot\eta_j^{\text{tag}\,2}<0\,, \tag{7a}$$

$$\eta_j^{\text{tag}\,1}+0.7<\eta_{\ell}<\eta_j^{\text{tag}\,2}-0.7$$

or (7b)

$$\eta_j^{\text{tag}\,2}+0.7<\eta_{\ell}<\eta_j^{\text{tag}\,1}-0.7.$$

Finally, the jet p_T distributions of Fig. 2(c) suggest a more stringent transverse-momentum requirement on the tagging jets as another means of enhancing the signal with respect to the background. We find that a cut at 70 GeV would be optimal for the significance of the signal. However, such a high cut would take us well outside the acceptable range for double jet tagging of weak-boson scattering events. The incident longitudinally polarized weak bosons in $qq\to qqH$ events lead to substantially lower transverse momenta of the tagging jets than the transversely polarized incident W's in the Zjj signal (median $p_T\approx 30$ GeV vs ≈ 70 GeV for the softer of the two tagging jets). Since we want to explore events which are as similar as possible to longitudinal weak-boson scattering events, we compromise at

$$p_{Tj}^{\text{tag}}>40\ \text{GeV}. \tag{8}$$

The resulting cross sections, after the cuts of Eqs. (4)–(8), are given in the second row of Table I. Distributions in dijet invariant mass and lepton-jet separation are shown in Fig. 3. These distributions show clearly that the QCD Zjj background can be further suppressed with respect to the signal, e.g., by increasing m_{jj}, the dijet invariant mass of the two tagging jets, or by requiring a larger minimal separation,

$$\Delta\eta_{\ell j}=\min_{\ell,j}\{|\eta_{\ell}-\eta_j^{\text{tag}}|\}, \tag{9}$$

between the Z decay leptons and the two tagging jets. Cross sections and signal to background ratios for three examples of more stringent cuts are shown in the last three rows of Table I; it will be possible to prepare event samples with very different fractions of electroweak- and QCD-induced Zjj events. The availability of both signal- and background-dominated event samples then will allow the study of radiation patterns of minijets in both t-channel color-singlet exchange events (signal) and in events which are due to color exchange between the incident partons (QCD background).

With regard to the separation of signal and QCD background, it also should be noted that the calculation of full NLO QCD corrections is possible for the Zjj signal with presently available techniques. Our calculation of gluon emission in $qQ\to qQZ$ (and all crossing related processes) constitutes already a full determination of the real emission corrections which contribute to the signal cross section at NLO. Since the signal involves t-channel color singlet exchange only, 1-loop amplitudes with t-channel gluon exchange do not interfere with the Born amplitude and, as a result, the most complicated Feynman graphs to be consid-

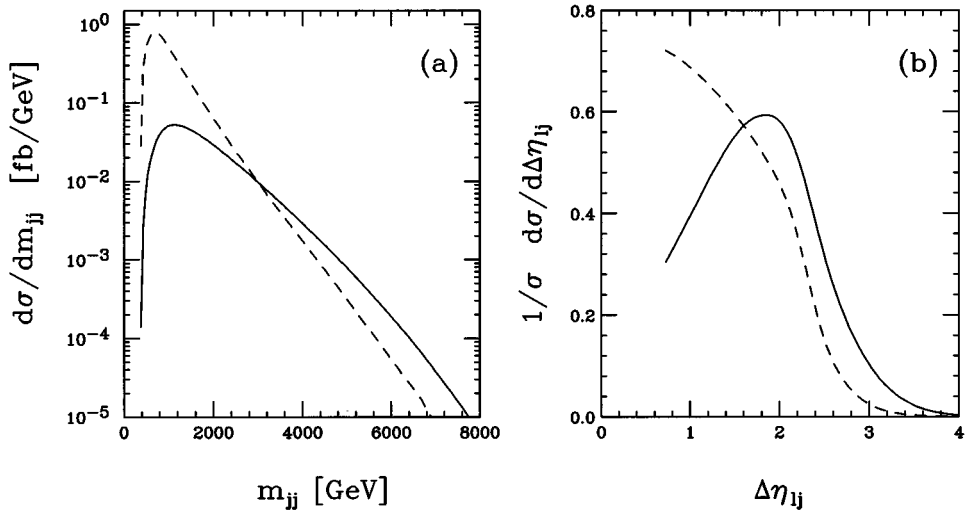

FIG. 3. Lepton and jet distributions of signal (solid lines) and background (dashed lines) Zjj events within the cuts of Eqs. (4)–(8). Shown are (a) the dijet mass distribution of the two tagging jets and (b) the minimal pseudorapidity separation $\Delta\eta_{lj}$ between any of the leptons and tagging jets. Note that the distribution in pseudorapidity separation has been normalized to unit area.

ered for the virtual corrections are box diagrams. Thus it can be reasonably expected that a NLO calculation of the signal cross section will be available by the time these measurements can be performed at the CERN LHC. Given the measured event rate and the predicted signal rate, the composition of the Zjj events should be known at the 10% level or better. Shape differences of distributions, as in Fig. 3, then can be used to verify the relative composition of event samples.

IV. RADIATION PATTERNS OF MINIJETS

Having isolated a phase-space region similar to the one populated by weak-boson scattering events, one can use two-jet inclusive Z production events to study the soft-jet activity in events with or without color exchange in the t channel. As discussed in Sec. II, we simulate the minijet activity in hard Zjj events by generating $Z+3$-parton signal and background events. In the presence of three jets, the tagging jets now are defined as the two most energetic jets with $p_T^{\rm tag}>40$ GeV in opposite hemispheres of the detector. In the following we are interested in the properties of the third or soft parton, which may or may not qualify as a minijet.

The pseudorapidity and transverse-momentum distributions of this third jet are shown in Fig. 4, where the p_{Tj} threshold has been lowered to 10 GeV. As expected for t-channel color-singlet exchange, additional jet activity in the signal is concentrated in the forward and backward regions. Color exchange between the incident partons, as in the case of the QCD background, leads to minijet activity in the central region. These differences become particularly pronounced when measuring the soft jet's rapidity with respect to the center of the two tagging jets, i.e., by using the shifted pseudorapidity

$$\eta_3^* = \eta_3 - \overline{\eta} = \eta_3 - \frac{\eta_j^{\rm tag\,1} + \eta_j^{\rm tag\,2}}{2}. \qquad (10)$$

The dip in Fig. 4(a) at $\eta_3^*=0$ is the hallmark of color coherence in color-singlet exchange [4,20,21]. Beyond this different angular distribution of the soft-jet activity, another striking difference arises in the transverse-momentum distribution of the third jet; the additional jet is substantially harder in the QCD background than in the signal. This difference is hardly noticeable in the shape of the p_{T3} distribution. It becomes apparent, however, by integrating the $Zjjj$ cross section above a given minimum transverse momentum, $p_{T,\rm min}$, of the nontagging jet,

$$\sigma_3 = \sigma(p_{T3} > p_{T,\rm min}) = \int_{p_{T,\rm min}}^{\infty} \frac{d\sigma}{dp_{T3}} dp_{T3}. \qquad (11)$$

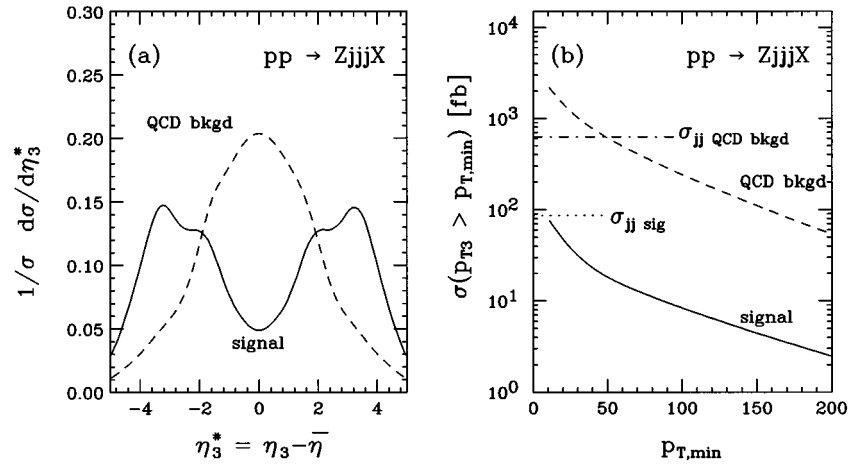

FIG. 4. Characteristics of the third (soft) jet in $Zjjj$ signal (solid lines) and background (dashed lines) events at the LHC. (a) The pseudorapidity η_3^* is measured with respect to the center of the two tagging jets, $\overline{\eta}=(\eta_j^{\rm tag\,1}+\eta_j^{\rm tag\,2})/2$, and the distributions are normalized to unit area. (b) Integrated transverse-momentum distribution of the third jet, $\sigma(p_{T3}>p_{T,\rm min})$. The acceptance requirements of Eqs. (4)–(8) are imposed on the two tagging jets. The corresponding cross sections at lowest order, with two partons in the final state, are indicated for the signal (dotted line) and for the background (dash-dotted line).

This integrated three-jet cross section, σ_3, is shown as a function of $p_{T,\min}$ and compared to the two-jet cross section, $\sigma_2=\sigma_{jj}$, in Fig. 4(b).

The number of events with two leptons and two tagging jets, which satisfy the cuts of Eqs. (4)–(8), will be clearly independent of the transverse momentum threshold $p_{T,\min}$. At tree level we must, therefore, interpret the Zjj cross section σ_2 as the two-jet inclusive cross section.[2] The alternative interpretation of $\sigma_2+\sigma_3$ as the two-jet inclusive cross section is unphysical since σ_3 can be made arbitrarily large by lowering $p_{T,\min}$.

As long as $\sigma_3(p_{T,\min})\ll\sigma_2$, fixed-order perturbation theory should be reliable, and we can expect cross sections for four or more jets to be small. Figure 4(b) demonstrates that, for the electroweak signal, this perturbative regime covers all p_T thresholds of practical interest; σ_3 saturates the two-jet inclusive cross section, σ_2, at $p_{T,\min}(\text{signal})=7.6$ GeV, and this value is well below the range where minijets from overlapping events become important; at design luminosity of $\mathcal{L}=10^{34}\ \text{cm}^{-2}\ \text{sec}^{-1}$, a random jet of $p_{Tj}\gtrsim 20$ GeV is expected in about 20% of all bunch crossings [22].

The situation is very different for the QCD background. Here $\sigma_3\approx\sigma_2$ is reached at $p_{T,\min}(\text{background})=41$ GeV. Clearly, fixed-order perturbation theory is breaking down for $p_{T,\min}\gtrsim 70$ GeV and large values of σ_4, σ_5, etc. must be expected. In the actual experiment multiple minijet emission will appear in this transverse-momentum range. Thus the t-channel color-singlet exchange of the signal and the color exchange of the QCD background lead to dramatically different minijet activity in individual events; color-singlet-exchange events will sport a low occupancy of fairly soft jets in the forward and backward region with very little activity in the central region, while a typical QCD background event will have several minijets of transverse momentum above 20 GeV, predominantly in the central region, between the the two tagging jets.

In the analogous case of weak-boson scattering events, the same pattern arises and a veto on central minijets can be used to suppress the backgrounds [5]. The efficiency of a minijet veto can be tested experimentally at the CERN LHC using the Zjj events discussed here. The precise definition of a minijet veto will depend on detector performance, multiplicity of minijets from overlapping events [22], and detailed signal and background characteristics. Given the characteristics of signal and background $Zjjj$ events discussed above, the veto region may be defined as the pseudorapidity range between the tangents to the two tagging jets, and as jet transverse momenta above a minimal value, $p_{T,\text{veto}}$,

$$p_{Tj}^{\text{veto}} > p_{T,\text{veto}}, \tag{12a}$$

$$\min\{\eta_j^{\text{tag }1},\eta_j^{\text{tag }2}\}+0.7<\eta_j^{\text{veto}}<\max\{\eta_j^{\text{tag }1},\eta_j^{\text{tag }2}\}-0.7, \tag{12b}$$

and we will use this definition as an example in the following.

Jets with transverse momentum in the 20 GeV range should be observable in hard events at the CERN LHC [22], and perhaps even lower thresholds are possible at luminosities below $\mathcal{L}=10^{33}\ \text{cm}^{-2}\ \text{sec}^{-1}$. Since, for the QCD background, this p_T range is below the validity region of fixed-order QCD, we need to resort to some modeling in order to estimate the probability for multiple minijet emission. Any model should preserve the two salient features of the QCD matrix-element calculation: color coherence as reflected by the angular distributions of Fig. 4(a) and the different p_T scales for extra parton emission that we have found for the signal and the background.

In the following we use the two models discussed in Ref. [5]. The first one is provided by the ''truncated shower approximation'' (TSA) [23]. When several soft gluons are emitted in a hard scattering event, their transverse momenta tend to cancel, leading to a regularization of the small p_T singularity which is present when considering only single-parton emission. In the TSA these effects are simulated by replacing the tree-level three-jet differential cross section $d\sigma_3^{\text{TL}}$ with

$$d\sigma_3^{\text{TSA}}=d\sigma_3^{\text{TL}}(1-e^{-p_{T3}^2/p_{\text{TSA}}^2}). \tag{13}$$

Here the parameter p_{TSA} is chosen to reproduce correctly the tree-level two-jet cross section, σ_2, within the cuts of Eqs. (4)–(8), i.e., p_{TSA} is fixed by the matching condition

$$\sigma_2=\int_0^\infty \frac{d\sigma_3^{\text{TSA}}}{dp_{T3}}dp_{T3}. \tag{14}$$

This is achieved by setting $p_{\text{TSA}}=10.5$ GeV for the Zjj signal and $p_{\text{TSA}}=72$ GeV for the QCD Zjj background. The much larger value for the latter again reflects the higher intrinsic momentum scale governing soft-gluon emission in the QCD background. This difference would be enhanced even more by requiring larger dijet invariant masses for the two tagging jets, as in the final two rows of Table I (see also below). Using $d\sigma_3^{\text{TSA}}$ as a model for additional jet activity, we find the probabilities of Fig. 5 (dotted and dash-dotted curves) for emission of a third, soft parton into the veto region of Eq. (12).

In the TSA only one soft parton is generated, with a finite probability to be produced outside the veto region of Eq. (12b). The veto probability will, therefore, never reach 1, no matter how low a $p_{T,\text{veto}}$ is allowed. At small values of $p_{T,\text{veto}}$ we underestimate the veto probability because the TSA does not take into account multiple parton emission. In the soft region gluon emission dominates, and one may assume that this soft-gluon radiation approximately exponentiates, i.e., the probability P_n for observing n soft jets in the veto region is given by a Poisson distribution,

$$P_n=\frac{\overline{n}^n}{n!}e^{-\overline{n}}, \tag{15}$$

with

[2]Here and in the following we use the term ''n-jet inclusive cross section'' to count the number of events with n or more jets, i.e., each event is counted once, independent of the jet multiplicity in the event.

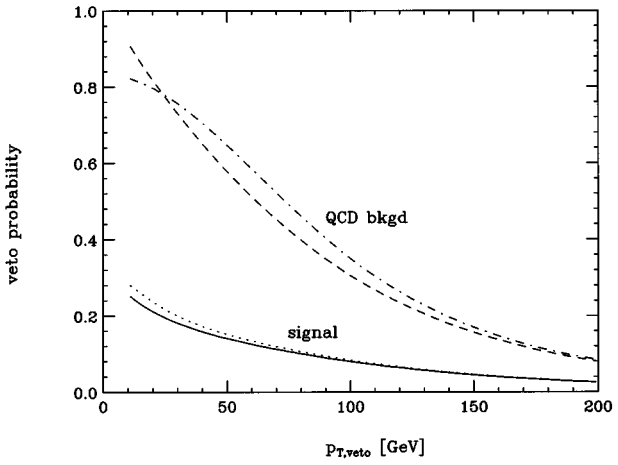

FIG. 5. Probability to find a veto jet with transverse momentum above $p_{T,\mathrm{veto}}$ and in the pseudorapidity range of Eq. (12b) in signal and background events within the cuts of Eqs. (4)–(8). The solid (signal) and dashed (background) curves are obtained with the exponentiation ansatz of Eq. (15) while the truncated shower approximation yields the dotted curve for the signal and dash-dotted curve for the QCD background.

$$\overline{n} = \overline{n}(p_{T,\mathrm{veto}}) = \frac{1}{\sigma_2}\int_{p_{T,\mathrm{veto}}}^{\infty} dp_{T3}\frac{d\sigma_3}{dp_{T3}}, \tag{16}$$

where the unregularized three-parton cross section is integrated over the veto region of Eq. (12) and then normalized to the Zjj cross section, σ_2. We will call this model the ''exponentiation model.'' A rough estimate of multiple emission effects is thus provided by using

$$P_{\exp}(p_{T,\mathrm{veto}}) = 1 - P_0 = 1 - e^{-\overline{n}(p_{T,\mathrm{veto}})} \tag{17}$$

for the veto probability. The resulting curves are the solid and dashed lines in Fig. 5. In spite of the approximations made, both models agree qualitatively on the much larger probability to observe additional minijets in the QCD background as compared to the Zjj signal.

Within the exponentiation model, $\overline{n} = \sigma_3/\sigma_2$ represents the average multiplicity of minijets in the central region, between the two tagging jets. Even if the exponentiation model is only of limited accuracy, the ratio of three- to two-jet tree-level cross sections gives the best perturbative estimate available of the minijet activity in Zjj events. One finds that the average minijet multiplicity depends strongly on the hardness of the underlying Zjj event. In Figs. 6(a) and 6(b) the dependence of $\overline{n}$ on the dijet invariant mass of the two tagging jets is shown for both the signal and the QCD background, for four values of the transverse-momentum cut on minijets: $p_{T,\mathrm{veto}} = 10$ GeV (solid line), 20 GeV (dashed line), 40 GeV (dotted line), and 80 GeV (dash-dotted line). The differential cross sections $d\sigma/dm_{jj}$ are shown in Figs. 6(c) and 6(d), allowing an assessment of the relative importance of regions of different $\overline{n}$.

Except for the threshold region, where kinematical effects of additional minijet emission are most important, the minijet multiplicity in signal events is below 25% everywhere, and thus fixed-order perturbation theory should be reliable. Perhaps somewhat surprisingly, the minijet activity of the signal decreases with increasing m_{jj}. This effect can be traced to the relative contribution of gluon-initiated $gQ \to q\overline{q}QZ$ events as compared to events with soft gluons in the final state, $qQ \to qQZg$. The splitting process $g \to q\overline{q}$ has a much higher probability to produce a semihard central jet than gluon radiation in t-channel color-singlet exchange. In the latter case color coherence between initial- and final-state radiation forces the gluon jet into the forward and backward regions [4], and in addition the transverse-momentum spectrum of the produced gluon is much softer than that of the additional quark jet in $g \to q\overline{q}$ splitting. By themselves, $qQ \to qQZg$ events would produce an essentially flat minijet multiplicity distribution, which, for $p_{T3} > 20$ GeV, varies between $\overline{n} = 0.16$ and $\overline{n} = 0.12$ over the entire m_{jj} range shown in Fig. 6(a). Since high m_{jj} events populate the large Feynman-x region, where the valence-quark distributions dominate, the pattern expected for final-state gluons is found when concentrating on the high-invariant-mass region.

The situation is entirely different for high-mass QCD background events, which are dominated by t-channel gluon exchange. The relevant scale for the acceleration of color charges and, hence, the emission of soft gluons, is set by m_{jj}, and, as a result, the minijet multiplicity in Fig. 6(b) increases substantially with rising invariant mass of the two tagging jets. In addition the expected minijet multiplicity is about an order of magnitude higher in QCD background events than in the Zjj signal. This different dependence of $\overline{n}$ on m_{jj} has an intriguing consequence: plotting the minijet multiplicity distribution of Zjj data in increasingly higher m_{jj} bins, one expects a clear separation to develop between the signal events, which will be concentrated at zero minijet multiplicity, and the QCD background events, which will populate the high-multiplicity region.

The emission of additional partons depends above all on the energy scale of the underlying hard process. The minijet multiplicity shows much less variation with angular variables. One example is given in Fig. 7 where the dependence of $\overline{n}$ on the minimal separation $\Delta\eta_{\ell j}$ of the Z-decay leptons from the two tagging jets is shown. For separations below ≈ 2.2, where both signal and background cross sections are sizable, $\overline{n}$ is essentially independent of $\Delta\eta_{\ell j}$. Given the different shapes of $d\sigma/d\Delta\eta_{\ell j}$, a statistical separation of signal and QCD background may be possible for events with any given number of minijets. This would allow the independent measurement of the minijet multiplicity distributions for t-channel color-singlet exchange and QCD background events, thus providing important input for weak-boson scattering events and their backgrounds in basically the same kinematical regime.

Before closing this section, let us consider briefly some of the uncertainties of our LO calculation. Motivated by the observation of rather high minijet activity in hard dijet events at the Tevatron [24], we have chosen a small scale and thus a large value of α_s to model the minijet multiplicity, $\overline{n}$ [25]. The choice of a larger scale reduces the predicted minijet multiplicity, in particular for low minijet transverse momentum thresholds ($p_{T3} > 10$ or 20 GeV) and for large values of m_{jj}. Taking the transverse mass of the produced Z boson as the factorization and renormalization scales lowers the average $\overline{n}$ by about 30% for the signal and 20% for the background when considering $p_{T3} > 10$ GeV, and these numbers

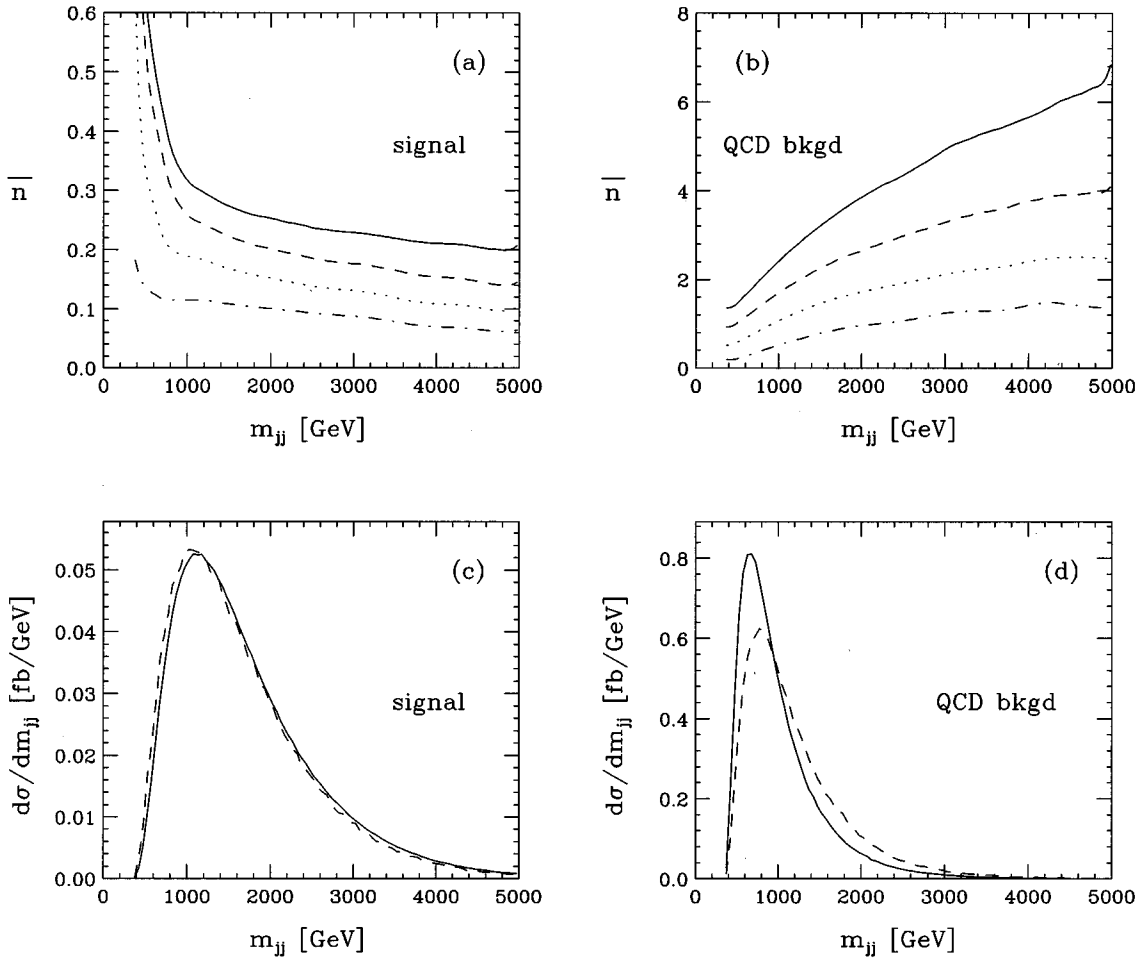

FIG. 6. Average minijet multiplicity $\overline{n}=\sigma_3(p_{T,\min})/\sigma_2$ in the veto region of Eq. (12) as a function of the invariant mass of the two tagging jets, m_{jj}, for four different transverse momentum thresholds of the third jet: $p_{T,\text{veto}}=10$ GeV (solid line), 20 GeV (dashed line), 40 GeV (dotted line), and 80 GeV (dash-dotted line). Results are shown for (a) the Zjj signal and (b) the QCD background. Below each, $d\sigma/dm_{jj}$ is shown as determined with Zjj tree-level matrix elements (solid lines) and by using the truncated shower approximation (dashed lines).

reduce to 20% and 10%, respectively, for a minijet threshold of $p_{T3}>20$ GeV. For the signal we are still in the perturbative region and, therefore, we expect these numbers to represent a realistic estimate of the uncertainties of our calculation. Given the assumptions which go into the exponentiation model, the error for the background numbers might well be substantially larger and our calculation only provides a rough estimate for the minijet multiplicity. This is exactly why a direct measurement at the CERN LHC is needed.

V. DISCUSSION

The production of Zjj events at the CERN LHC, with one forward and one backward tagging jet which are widely separated in pseudorapidity, provides an ideal testing ground for the study of t-channel color-singlet exchange events. The electroweak process $qq\to qqZ$ possesses all the relevant characteristics of weak-boson scattering events. However, it is easily identifiable via the leptonic Z-decay mode, and it enjoys a large production cross section (of order 30–80 fb) in a phase-space region where QCD backgrounds are of comparable size. Even when operating the CERN LHC at 10% of the design luminosity (i.e., collecting 10 fb^{-1} per year) a combined signal and background sample of more than 1000 events will be available to find differences between events with and without color exchange in the t channel. By varying the machine luminosity, the minijet background from overlapping events in the same bunch crossing, and methods for its suppression, can be studied at the same time [22].

Color-singlet exchange in the t channel, as encountered in Higgs-boson production by weak-boson fusion and in our Zjj signal, leads to soft-minijet activity which differs strikingly from that expected for the QCD backgrounds in at least two respects. First, t-channel color-singlet exchange leads to soft-gluon emission mainly in the forward and backward regions, between the beam directions and the forward tagging jets [4,21]. The central region between the two tagging jets, which also contains the two Z-decay leptons, remains largely free of minijets. For the backgrounds, t-channel color exchange leads to minijet emission mainly in the central region [5].

A second distinction is the typical transverse momentum of the produced minijets. Extra gluon emission in Zjj production is suppressed by a factor $f_s=\alpha_s\ln(Q^2/p_{T,\min}^2)$, where

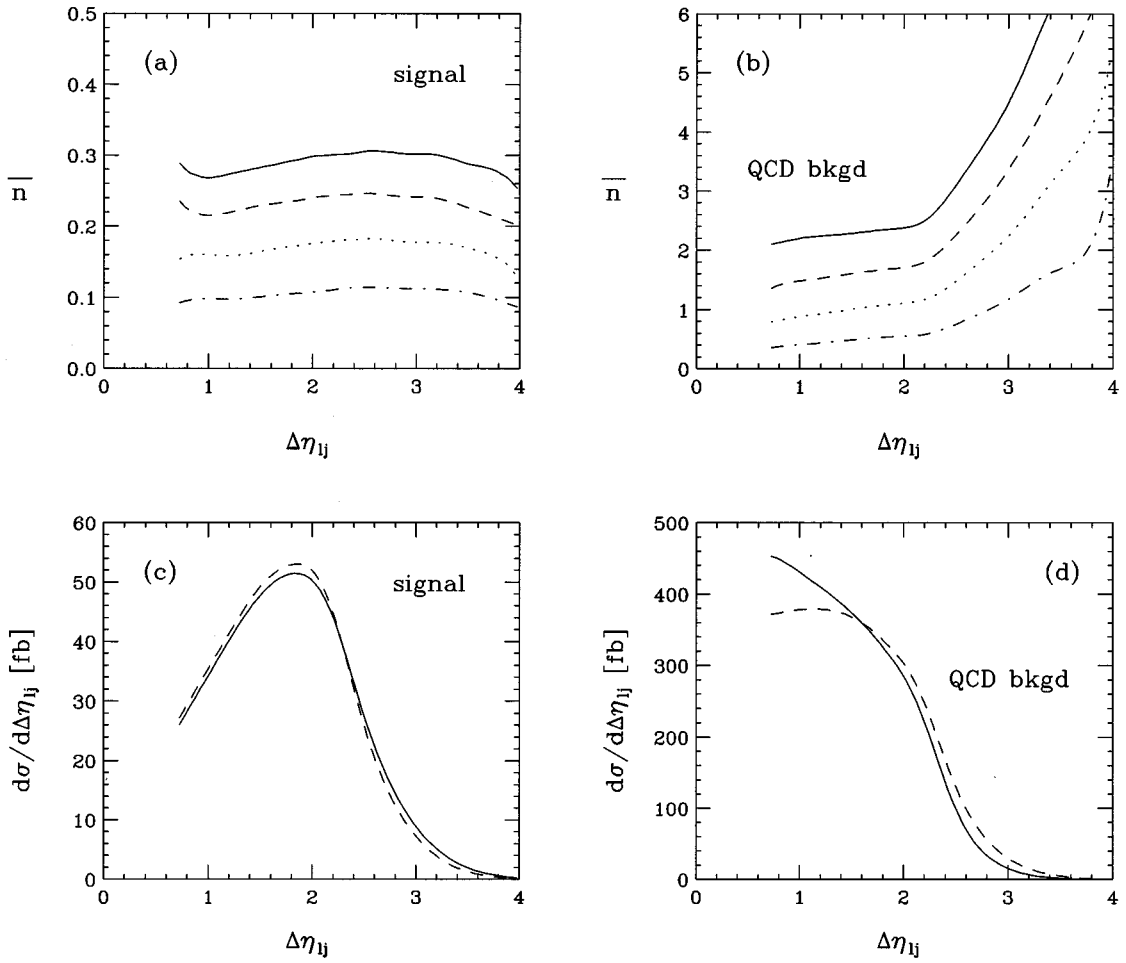

FIG. 7. Same as Fig. 6, but for the dependence of the minijet activity on the minimal separation $\Delta\eta_{\not\ell j}$ of the Z-decay leptons from the two tagging jets. See text for details.

Q is the typical scale of the hard process and $p_{T,\min}$ is the minimal transverse momentum required for a parton to qualify as a minijet. The jet-transverse-momentum scale below which multiple minijet emission must be expected is set by $f_s \approx 1$. The hard scale Q is set by the momentum transfer to the color charges in Zjj production. For the signal no color is exchanged, and, hence, the color charges are accelerated by the same amount as the incoming (anti)quarks. Hence, Q is related to the average p_T of the two tagging jets and is only of order 100 GeV. For the background processes, on the other hand, color is exchanged in the annihilation of the initial quarks and/or gluons. Therefore the momentum transfer to the color charges is of the order of the dijet invariant mass of the two tagging jets and is in the TeV range. As a result multiple minijet emission becomes important in background processes in the 20–50 GeV p_T range whereas the corresponding scale for the signal is only of order a few GeV [5].

These qualitative arguments are directly confirmed by our perturbative analysis. We find, for example, that minijet emission in the QCD background increases with the invariant mass of the two tagging jets, and that it occurs with much higher probability than for the signal even though the transverse momenta of the tagging jets are somewhat larger in the electroweak Zjj signal than in the QCD background. This pattern is naturally explained by taking $Q = m_{jj}$ for the background and $Q = p_{Tj}^{\text{tag}}$ for the signal.

A precise modeling of multiple minijet emission in hard QCD processes is beyond the scope of the present paper. However, any Monte Carlo program which addresses this question should incorporate the above findings and agree with the fixed-order perturbation-theory results at sufficiently large minijet transverse momenta. Zjj events at the CERN LHC then can be used to fine-tune the Monte Carlo programs in the low p_T range.

Because of its intrinsically small scale, fixed-order QCD should be reliable for the signal process down to minijet transverse momenta in the 10–20 GeV range, a point which can be tested experimentally by comparing the rate of low minijet multiplicity $Z+2$-jet inclusive events with the signal predictions (to NLO if available by the time the CERN LHC starts running).

Minijet activity in high-mass QCD events is most easily probed by studying two-jet inclusive events (without an accompanying Z boson), as is already possible now, at the Tevatron [24,25]. However, such events will have a composition of quark- and gluon-initiated subprocesses different from backgrounds to weak-boson scattering events. A test run to prepare for the latter can be performed with the Zjj QCD backgrounds studied here. Samples of such events can

be prepared either by subtracting the known electroweak Zjj production cross section, by relying on differing shapes of kinematical distribution at the $Z+2$-jet level, or by going to relatively low dijet-mass regions where the QCD Zjj background is the dominant source of Zjj events.

Most likely a combination of all of these will be needed to obtain an understanding of the minijet activity in hard scattering events at a quantitative level. This knowledge then can be used to devise a minijet trigger for the Higgs-boson search at the CERN LHC. Our findings here indicate that a minijet veto should work not only for the heavy Higgs-boson search, where the production of a high-mass system lets one expect strong gluon radiation in background events, but also for the production of light weak bosons via WW or ZZ fusion. This weak boson need not be the Z studied here, but could be an intermediate-mass Higgs boson. The use of a minijet veto appears to be a promising technique for the entire Higgs mass range, from the 100 GeV range of supersymmetric models to the TeV scale.

ACKNOWLEDGMENTS

We thank Tim Stelzer for his aid in testing our matrix elements by a comparison with MadGraph. This research was supported in part by the University of Wisconsin Research Committee with funds granted by the Wisconsin Alumni Research Foundation and in part by the U.S. Department of Energy under Contract No. DE-FG02-95ER40896.

[1] R. N. Cahn *et al.*, Phys. Rev. D **35**, 1626 (1987); V. Barger, T. Han, and R. J. N. Phillips, *ibid.* **37**, 2005 (1988); R. Kleiss and W. J. Stirling, Phys. Lett. B **200**, 193 (1988); D. Froideveaux, in *Proceedings of the ECFA Large Hadron Collider Workshop*, Aachen, Germany, 1990, edited by G. Jarlskog and D. Rein (CERN Report No. 90-10, Geneva, Switzerland, 1990), Vol. II, p. 444; M. H. Seymour, *ibid.*, p. 557; U. Baur and E. W. N. Glover, Nucl. Phys. **B347**, 12 (1990); Phys. Lett. B **252**, 683 (1990).

[2] V. Barger *et al.*, Phys. Rev. D **42**, 3052 (1990); V. Barger *et al.*, *ibid.* **44**, 1426 (1991); V. Barger *et al.*, *ibid.* **44**, 2701 (1991); erratum, *ibid.* **48**, 5444 (1993); *ibid.* **48**, 5433 (1993); V. Barger *et al.*, *ibid.* **46**, 2028 (1992).

[3] D. Dicus, J. F. Gunion, and R. Vega, Phys. Lett. B **258**, 475 (1991); D. Dicus, J. F. Gunion, L. H. Orr, and R. Vega, Nucl. Phys. **B377**, 31 (1991).

[4] Y. L. Dokshitzer, V. A. Khoze, and S. Troyan, in *Proceedings of the Sixth International Conference on Physics in Collisions*, 1986, edited by M. Derrick (World Scientific, Singapore, 1987), p. 365; J. D. Bjorken, Int. J. Mod. Phys. A **7**, 4189 (1992); Phys. Rev. D **47**, 101 (1993).

[5] V. Barger, R. J. N. Phillips, and D. Zeppenfeld, Phys. Lett. B **346**, 106 (1995).

[6] K. Hagiwara and D. Zeppenfeld, Nucl. Phys. **B313**, 560 (1989).

[7] V. Barger, T. Han, J. Ohnemus, and D. Zeppenfeld, Phys. Rev. Lett. **62**, 1971 (1989); Phys. Rev. D **40**, 2888 (1989).

[8] F. A. Berends, W. T. Giele, H. Kuijf, R. Kleiss, and W. J. Stirling, Phys. Lett. B **224**, 237 (1989).

[9] H. Chehime and D. Zeppenfeld, Phys. Rev. D **47**, 3898 (1993).

[10] U. Baur and D. Zeppenfeld, in *Proceedings of the Workshop on Physics at Currect Accelerators and Supercolliders*, Argonne, Illinois, edited by J. L. Hewett, A. R. White, and D. Zeppenfeld (Argonne Report No. ANL-HEP-CP-93-92, Argonne, 1994), p. 327.

[11] K. Hagiwara and D. Zeppenfeld, Nucl. Phys. **B274**, 1 (1986).

[12] T. Stelzer and W. F. Long, Comput. Phys. Commun. **81**, 357 (1994).

[13] A. Duff and D. Zeppenfeld, Phys. Rev. D **50**, 3204 (1994).

[14] A. D. Martin, R. G. Roberts, and W. J. Stirling, Phys. Rev. D **50**, 6734 (1994).

[15] H. Plothow-Besch, Int. J. Mod. Phys. A **10**, 2901 (1995); H. Plothow-Besch, PDFLIB: Nucleon, Pion and Photon Parton Density Functions and α_s Calculations, Users's Manual-Version 6.06, W5051 PDFLIB, 1995.03.15, CERN-PPE (unpublished).

[16] H. L. Lai *et al.*, Phys. Rev. D **51**, 4763 (1995).

[17] T. Han, G. Valencia, and S. Willenbrock, Phys. Rev. Lett. **69**, 3274 (1992).

[18] S. D. Ellis, R. Kleiss, and W. J. Stirling, Phys. Lett. **154B**, 435 (1985); R. Kleiss and W. J. Stirling, Nucl. Phys. **B262**, 235 (1985); Phys. Lett. B **180**, 171 (1986); J. F. Gunion, Z. Kunszt, and M. Soldate, Phys. Lett. **163B**, 389 (1985); erratum, *ibid.* **168B**, 427 (1986); J. F. Gunion and M. Soldate, Phys. Rev. D **34**, 826 (1986); R. K. Ellis and R. J. Gonsalves, in *Supercollider Physics, Proceedings of the Workshop on Super High Energyy Physics*, Eugene, Oregon,1985, edited by D. E. Soper (World Scientific, Singapore, 1986), p. 287.

[19] W. W. Armstrong *et al.*, Atlas Technical Proposal, Report No. CERN/LHCC/94-43, 1994 (unpublished). G. L. Bayatian *et al.*, CMS Technical Proposal, Report No. CERN/LHCC/94-38, 1994 (unpublished).

[20] Y. L. Dokshitzer *et al.*, Rev. Mod. Phys. **60**, 373 (1988), and references therein.

[21] R. S. Fletcher and T. Stelzer, Phys. Rev. D **48**, 5162 (1993).

[22] G. Ciapetta and A. DiCiaccio, in *Proceedings of the ECFA Large Hadron Collider Workshop* [1], Vol. III, p. 155.

[23] V. Barger and R. J. N. Phillips, Phys. Rev. Lett. **55**, 2752 (1985); H. Baer, V. Barger, H. Goldberg, and R. J. N. Phillips, Phys. Rev. D **37**, 3152 (1988).

[24] CDF Collaboration, F. Abe *et al.*, Phys. Rev. Lett. **75**, 608 (1995); D0 Collaboration, John Womersley, presented at the 11th Topical Workshop on Proton-Antiproton Collider Physics, Padua, Abano Terme, Italy, 1996 (unpublished).

[25] D. Summers and D. Zeppenfeld, Phys. Lett. B **380**, 426 (1996).